A COMPARISON OF IDES MODEL PREDICTIONS WITH DEBRIS MEASUREMENT DATA

R. Walker, R. Crowther, V. Marsh, H. Stokes

Space Department, Defence Research Agency, Farnborough, Hants., GU14 0LX, UK

G.G. Swinerd

Department of Aeronautics & Astronautics, University of Southampton, Hants., SO17 1BJ, UK

ABSTRACT

Orbital debris models are essential for characterising the entire debris environment, especially for orbit and size regimes where measurements have poor coverage. Models are required to provide an accurate assessment of collision risk to current and future missions. The accuracy of the IDES model over a wide range of debris sizes is evaluated by comparing model predictions to three major types of debris measurement data. These are the tracked debris population of large-size debris, radar detections of mid-size debris, and small-size debris impact fluxes inferred from space returned surfaces. For the tracked population, direct comparison of spatial densities is applied. For comparisons with radar detection data, a radar simulation model is used to predict the detection rates of debris in a field of view. Finally, a collision risk analysis is performed to predict the impact flux relative to a retrieved spacecraft.

1. INTRODUCTION

The ultimate test of any simulation model is a comparison with the real world that the model is designed to represent. For a model such as IDES, this validation process should compare model predictions with reliable measurements of the population. Validation is essential in determining the accuracy of the model and can serve to enhance accuracy for future model developments. Confidence in the model predictions, particularly for simulating future debris evolution where no comparison with measurement data is possible, is strongly dependent upon a rigorous validation programme.

The most deterministic debris measurement data available is currently the US Space Command (USSPACECOM) catalog which contains the orbital elements of over 8000 Earth orbiting objects tracked by ground sensors. The catalog data is suitable for validating the debris source and sink models of environment simulation models such as IDES, including the breakup and orbit perturbation models. The USSPACECOM catalog contains data on decimetre-sized objects and larger in low Earth orbit (LEO) and can also be used to validate the modelled environment above this size threshold. Two of the most reliable sources of measurement data for the smaller sized untrackable debris population are the detections of the US Haystack ground radar (ref. 1) and the impact analysis of the retrieved Long Duration Exposure Facility (LDEF) spacecraft (ref. 2). These measurements are used to validate the IDES prediction of the mid to small-sized debris population.

Haystack has been statistically sampling the LEO environment of debris larger than 1 cm since 1990 by counting the number of objects passing through its radar beam which is operated in various fixed orientation 'beam-park' modes.

The LDEF spacecraft was exposed to the debris environment between 1984 and 1990 at an approximate operating altitude of 475 km and inclination of 28.5°. LDEF received a large number of debris and meteoroid impacts from micron to millimetre sized particles. The impact sites were counted and analysed upon return to Earth, thus revealing the directionality and magnitude of debris flux encountered at various impactor sizes.

2. THE IDES MODEL

The Defence Research Agency's Integrated Debris Evolution Suite (IDES) has been developed in order to model the historical, current and possible future orbital debris environments in LEO, and to provide directional collision risk assessments for individual orbiting satellites. Ref. 3 provides more specific information on the IDES modelling techniques. The IDES model has been extensively developed and tested to ESA PSS-05 Software Engineering Standards. The results presented in this paper constitute part of the model validation/user acceptance testing of IDES required by these standards for product-level software.

The IDES current debris environment model on 1st January 1996 is characterised by simulating each of the past 133 recorded fragmentation events in space as either a low intensity explosion, a high intensity explosion, or a catastrophic collision and predicting the orbital evolution of all the generated fragments larger than 10 microns up to the reference epoch. IDES is

capable of modelling the major orbit perturbations for debris larger than 10 microns, which include geopotential, atmospheric drag, luni-solar and solar radiation pressure effects. Launch-related objects such as payloads, rocket upper stages, and operational debris from the USSPACECOM catalog are then added to the 1996 fragment population. IDES can also model secondary ejecta and paint flaking from meteoroid/debris impacts, but their contributions are not currently included in the results.

The evolving debris population in IDES has a split representation. Objects greater than a given size threshold are given their own specific attributes, such as an identifier, family code, orbital elements, mass and area. The size threshold is set to 10 cm in order to make comparisons with the trackable part of the population. The small-size debris population is represented by a fragment orbit matrix which stores the number of objects in the population discretised into bins by dimensions of perigee radius, eccentricity, inclination, and mass. This structure has the flexibility to add large numbers of objects as small as 10 microns from discrete breakup events and more continuous sources such as paint flaking. This representation is the same as that used by Madler in ref. 4, who also added size as a dimension. An earlier version of this matrix was employed by Rossi et al. for the SDM/STAT model in ref. 5. The STAT program binned the population by semi-major axis, eccentricity, and mass.

2.1 Orbit Perturbation Modelling

IDES propagates the orbits of individual large objects with respect to atmospheric drag, geopotential, luni-solar and solar radiation pressure perturbations. Small objects are binned by their values of perigee radius, eccentricity, inclination, and mass in a fragment orbit matrix. A Monte Carlo propagation technique propagates a number of weighted particles with randomly sampled orbits from each orbit-mass bin with respect to atmospheric drag, luni-solar, and solar radiation pressure perturbations over a timestep, Δt. Each weighted particle represents a certain number of real objects and this number is added to the respective orbit bin location corresponding to the new orbital elements in a new fragment orbit matrix for epoch, $t+\Delta t$.

2.1.1 Geopotential Perturbations

The geopotential perturbation equations are summarised by Roy (ref. 6). The most important component of geopotential perturbations is that of first order J_2 (second harmonic) secular variations over time, Δt. The orbital elements that are constantly rotating are right ascension of the ascending node, Ω, and argument of perigee, ω, according to semi-major axis, a, eccentricity, e, inclination, i, semi-latus rectum, p, and Earth radius, R:

$$\overline{\Delta\Omega_{sec}} = -\frac{3}{2}\frac{J_2 R^2}{p^2}\bar{n}(\cos i)\Delta t \qquad (1)$$

$$\overline{\Delta\omega_{sec}} = \frac{3}{2}\frac{J_2 R^2}{p^2}\bar{n}\left(2-\frac{5}{2}\sin^2 i\right)\Delta t \qquad (2)$$

$$\text{where} \quad \bar{n} = n_0\left[1+\frac{3}{2}\frac{J_2 R^2}{p^2}\left(1-\frac{3}{2}\sin^2 i\right)\sqrt{1-e^2}\right]$$

$$\text{and} \quad n_0 = \sqrt{\frac{\mu}{a^3}}$$

Long-period oscillations in the elements due to the third harmonic, J_3, are also of significance to long-term evolution dynamics. Inclination for example, varies according to secular variations in argument of perigee:

$$\Delta i_{lp} = \frac{3}{2}\frac{n_0 J_3 R^3}{a^3}\frac{e}{\left(1-e^2\right)^3}\cos i\left(1-\frac{5}{4}\sin^2 i\right)\cos\omega\ \Delta t \qquad (3)$$

2.1.2 Atmospheric Drag

The extensive research of King-Hele (ref. 7) is used to compute changes in semi-major axis and eccentricity by analytical methods. IDES employs the CIRA (Cospar International Reference Atmosphere) of 1972 to give values of atmospheric density and density scale height, H, according to the perigee height of the object orbit and the exospheric temperature, T_{ex}, which is modulated by the 30-day mean solar flux at a wavelength of 10.7 cm, $F_{10.7}$:

$$T_{ex} = 1.15\,(\,379 + 3.24\,F_{10.7}\,) \qquad (4)$$

Solar flux and therefore the decay rate is modulated by the solar cycle, with maximum decay rate during solar maximum conditions. The $F_{10.7}$ data has been taken from NASA Goddard historical records and future predictions.

King-Hele has shown that for a spherically symmetric atmosphere, the changes in semi-major axis, and eccentricity according to object area, A, mass, M, atmospheric density at perigee, ρ_p, and drag coefficient, C_D, are given by:

$$\Delta a = -2\pi\,\frac{A.C_D}{M}a^2\rho_p\exp\left[a_0 - a - a_0 e_0\right]f_1(I_0,I_1,I_2,I_3) \qquad (5)$$

$$\Delta e = -2\pi\,\frac{A.C_D}{M}a\,\rho_p\exp\left[a_0 - a - a_0 e_0\right]f_2(I_0,I_1,I_2,I_3,I_4) \qquad (6)$$

The functions $f_1(I_0,I_1,I_2,I_3)$ and $f_2(I_0,I_1,I_2,I_3,I_4)$ are bessel functions of the first kind with argument of $z = ae/H$.

2.1.3 Luni-Solar Perturbations

IDES considers the luni-solar perturbation effects on all orbits intersecting LEO by using the theory developed by Cook (ref. 8). Cook derived analytical expressions for the rate of change of the orbital elements from luni-solar effects based upon Lagrange's planetary equations and astronomical parameters of the Sun and Moon:

$$\frac{de}{dt} = -\frac{15K}{2n} e\sqrt{1-e^2}\left[AB\cos 2\omega - \tfrac{1}{2}\left(A^2 - B^2\right)\sin 2\omega \right] \qquad (7)$$

$$\frac{di}{dt} = \frac{3KC}{4n\sqrt{1-e^2}}\left[A\left(2 + 3e^2 + 5e^2\cos 2\omega\right) + 5Be^2 \sin 2\omega \right] \qquad (8)$$

$$\frac{d\Omega}{dt} = \frac{3KC}{4n\sqrt{1-e^2}\,\sin i}\left[5Ae^2 \sin 2\omega + B\left(2 + 3e^2 - 5e^2\cos 2\omega\right)\right] \qquad (9)$$

$$\frac{d\omega}{dt} = \frac{3K}{2n}\sqrt{1-e^2}\left[5\left\{ AB\sin 2\omega + \tfrac{1}{2}\left(A^2 - B^2\right)\cos 2\omega \right\}\right.$$

$$-1 + \tfrac{3}{2}\left(A^2 + B^2\right) + \frac{5a}{2er_d}\left(1 - \tfrac{5}{4}\left(A^2 - B^2\right)\right)$$

$$\left.\left(A\cos\omega + B\cos\omega\right)\right] - \frac{d\Omega}{dt}\cos i \qquad (10)$$

where $K = \dfrac{G\,M_d}{r_d^3}$

Coefficients A, B, and C are determined by trigonometric functions that relate the orbit of the disturbing body to the satellite orbit. G is the gravitational constant, n is the mean orbital motion, M_d and r_d are the mass of and radius to the disturbing body.

2.1.4 Solar Radiation Pressure Perturbations

Many small size debris have high area-to-mass ratios and consequently their orbits are influenced by solar radiation pressure (SRP). Similar to the luni-solar perturbation theory, Cook (ref. 8) gives the rate of change of the orbital elements from SRP effects:

$$\frac{de}{dt} = \frac{3\sqrt{1-e^2}}{2n\,a} T_p \qquad (11)$$

$$\frac{di}{dt} = -\frac{3We\cos\omega}{2na\sqrt{1-e^2}} \qquad (12)$$

$$\frac{d\Omega}{dt} = -\frac{3We\sin\omega}{2na\sqrt{1-e^2}\,\sin i} \qquad (13)$$

$$\frac{d\omega}{dt} = -\frac{3\sqrt{1-e^2}}{2nae} S_p - \frac{d\Omega}{dt}\cos i \qquad (14)$$

where $S_p = F.l_1\left(i,\omega,\Omega,L,\varepsilon\right)$,

$$T_p = -F.l_2\left(i,\omega,\Omega,L,\varepsilon\right),$$

$$W = \frac{F}{2\cos\omega}.l_3\left(i,\omega,\Omega,L,\varepsilon\right) \quad \text{and}$$

$$F = -\frac{4.5\times10^{-6}\left(1+\beta\right)A}{M}$$

The equation for F was taken from ref. 6. β is the surface reflectivity coefficient (set to 0.5). Coefficients S_p, T_p and W are the components of perturbing force in the satellite-based reference frame. They are directly proportional to F and their trigonometric functions l_1, l_2 and l_3. The functions are influenced by the angular elements of the object orbit, the geometric mean longitude of the Sun, L, and the mean obliquity of the ecliptic, ε. The theory assumes that the effect of Earth's shadow is neglected.

2.2 Breakup Modelling

Breakups events can be classified into three categories: low intensity explosions; high intensity explosions; and catastrophic collisions. The modelling process determines the mass, size, and area of each fragment, the velocity imparted to each fragment, and the resulting orbit. The following relationships are supported by deterministic data and preserve mass conservation.

2.2.1 Mass to Size/Area Conversion

Object mass, M, is related to size, d, and area, A_{eff}, by:

$$M(kg) = \begin{cases} 46.81\,d^{2.26} & if\ d > 0.0062\,\mathrm{m} \\ 2094\,d^{3} & if\ d \le 0.0062\,\mathrm{m} \end{cases} \qquad (15)$$

$$M(\mathrm{kg}) = \begin{cases} 61.5\,A_{eff}^{1.13} & if\ A_{eff} > 3.0\times10^{-5}\,\mathrm{m}^2 \\ 3009\,A_{eff}^{1.5} & if\ A_{eff} \le 3.0\times10^{-5}\,\mathrm{m}^2 \end{cases} \qquad (16)$$

(derived from debris densities in ref. 9)

Objects of common mass have a spreading about the effective area which is modelled by sampling the actual object area from a lognormal distribution with mean, A_{eff} and standard deviation 0.8, suggested by Jehn in ref. 10.

2.2.2 Mass Distribution

The cumulative number of fragments, CN, greater than mass, m, are given for the different breakup catagories.

Low Intensity Explosion:

$$CN = \begin{cases} 171.\exp\left(-0.6514\sqrt{m.f_m}\right) & for\ \ m \ge 1.936kg\,/\,f_m \\ 869.\exp\left(-1.8215\sqrt{m.f_m}\right) & for\ \ m < 1.936kg\,/\,f_m \end{cases} \qquad (17)$$

(ref. 11)

f_m is the ratio of 1000 kg over the breakup mass M_t.

High intensity explosions:

$$CN = \begin{cases} 171.\exp\left(-0.6514\sqrt{m.f_m}\right) & for\ \ m \geq 1.936kg / f_m \\ 869.\exp\left(-1.8215\sqrt{m}.f_m\right) & for\ \ m < 1.936kg / f_m \\ + \\ 0.331\left(\dfrac{m}{0.5\,M_t}\right)^{-0.78} \end{cases} \qquad (18)$$

50% of the breakup mass follows the low intensity exponential law, and 50% of the breakup mass follows a power law. In this case, f_m is the ratio of 1000 kg over 50% of the breakup mass, M_t. The power law coefficients are derived from the maximum power measured in the SOCIT series of ground tests summarised in ref. 12.

Catastrophic Collisions (EMR>40J/g):

$$CN = A\left(\frac{m}{M}\right)^{-B} \qquad (19)$$

$$where\ B = 0.60 + 0.18P\left[\frac{EMR - 40}{EMR}\right],$$

$$A = 1.6290 - 1.6636B$$

$$and\ M = M_t + M_p$$

(ref. 12)

EMR is the impactor energy-to-target mass ratio. The projectile mass, M_p, is included in the breakup mass.

Damaging Collisions/Craterizations (EMR<40J/g):

$$CN = 0.4478\left(\frac{m}{M}\right)^{-0.7496} \qquad (20)$$

where $M = M_e + M_p$ and $M_e = k\,M_p\,v^2$

(ref. 13)

v is the impact velocity in km/s. The residual target mass is found by debiting the total ejected mass, M_e, from the original target mass, M_t.

2.2.3 Delta-Velocity Distribution

The delta-velocity, ΔV, imparted to a fragment of size, d, depends upon the type of breakup.

Explosions:

$$\log\ \Delta v_{peak} = -0.0676(\log d)^2 - 0.804(\log d) - 1.5 \qquad (21)$$

(ref. 14)

Δv_{peak} is the characteristic delta-velocity in km/s and d is the debris size in m.

Collisions:

$$\log\left(\Delta v_{peak}\right) = \begin{cases} 0.875 - 0.0676.\left(\log\dfrac{d}{d_m}\right)^2 & ,d > d_m \\ 0.875 & ,d \leq d_m \end{cases} \qquad (22)$$

$$d_m = \frac{\sqrt[3]{E_p}}{c} \quad ; \quad E_p = \frac{1}{2} M_p.v^2$$

(ref. 15)

Δv_{peak} is the characteristic delta-velocity in km/s. d_m is the cut-off diameter in metres, c is a coefficient of value 8×10^8 $kg^{1/3}s^{-2/3}m^{-2/3}$, and v is the impact velocity in m/s.

The above relationships determine characteristic or peak delta-velocities according to a particular size. The spreading of ΔV values for fragments of a constant mass is respected by a triangular spreading function (ref. 15).

3. COMPARISON METHODS

Validation of the IDES breakup model can be performed by simulating selected historical on-orbit fragmentations and then comparing the orbital distribution of modelled debris clouds with distributions of the actual debris clouds in the catalog. The orbit perturbation model is validated by comparing long-term orbital evolution predictions of stable catalogued objects with the variation in their measured orbital elements from historical catalog data.

During an historical evolution simulation, IDES determines the size-dependent debris flux in high resolution three-dimensional space (discretised by Earth radius, declination, and right ascension) at regular time intervals by a novel application of the Klinkrad flux determination and collision risk analysis methods (ref. 16). These historical flux snapshots are accessed in order to produce the model predictions of the environment for comparison with measurement data. Firstly, the IDES 1996 spatial density distribution of >10cm debris over LEO altitudes is determined and compared to the spatial density distribution from objects in the 1st January 1996 USSPACECOM catalog.

In order to compare the IDES model predictions >1 cm with Haystack radar measurements taken between 1991 and 1994, it is necessary to use a radar simulation model that can convert the IDES flux environment snapshot of 1st January 1993 into the number of debris objects per hour crossing the field of view of the Haystack radar beam. The field of view model developed by NASA to compare the EVOLVE model with Haystack data is

used here (ref. 1). The radar beam in a 'zenith staring' (vertical) mode is divided into 5 km range intervals from 350 km to 1250 km. In the vertical mode, the beam traverses a line of constant latitude (and therefore constant declination in the IDES flux environment - a control volume divided into cells of Earth radius and declination) equal to the latitude of the Haystack site (42.6° N). The centre of each range interval is a 'detection site' which lies within a particular radius-declination cell of the IDES control volume containing a number of debris flux vectors. Each debris flux vector consists of a spatial density and a velocity vector with magnitude, azimuth and elevation in the cell reference frame.

The velocity magnitude perpendicular to the beam (ie. the velocity tangential to the radius shell) is determined and multiplied by the spatial density to obtain the debris flux of that vector crossing the beam. After a summation from all debris flux vectors in the cell, the total flux perpendicular to the detection site is multiplied by the perpendicular cross-sectional area of the beam range interval and the unit time is adjusted to 1 hour. The resulting value is the detection rate (the number of debris detected per hour) for a given range interval, assuming Haystack has a 100% probability of detection for debris of 1 cm and larger. The distribution of detection rate over all 5 km range intervals is then averaged every 50 km and directly compared to the Haystack data.

The historical flux environment snapshots output at 6 monthly time intervals between 1984 and 1990 are utilised by the IDES risk assessment program in order to predict the average cumulative debris flux relative to the LDEF orbit for 7 logarithmic size thresholds of 10 microns to 1 mm. In each snapshot, the debris flux vectors encountered in the volume cells intersected by the orbit are transformed into relative flux vectors in the spacecraft-centred moving reference frame (ref. 16). The relative flux vectors are weighted by the residential probability of the orbit in the respective intersected cells and summed to obtain the orbit-integrated mean relative flux for each size threshold. After averaging the size-dependent relative flux over the whole mission duration, the predictions can be compared with the measurements given in ref. 2.

4. COMPARISON RESULTS

For the validation of the IDES orbit perturbation model, we have chosen two examples of stable tracked orbits from the USSPACECOM catalog data between 1993 and 1996. In both cases, the initial orbital elements from the 1993 catalog were used as initial conditions for the perturbation model. Firstly, the Ariane 4-40 third stage (COSPAR ID 1991-050F) used to launch ERS-1 was selected as a representative debris object in a high inclination low Earth orbit. The area-to-mass ratio is well known, thus any error in the predictions are due to the perturbation theory, atmospheric model, and solar flux data only.

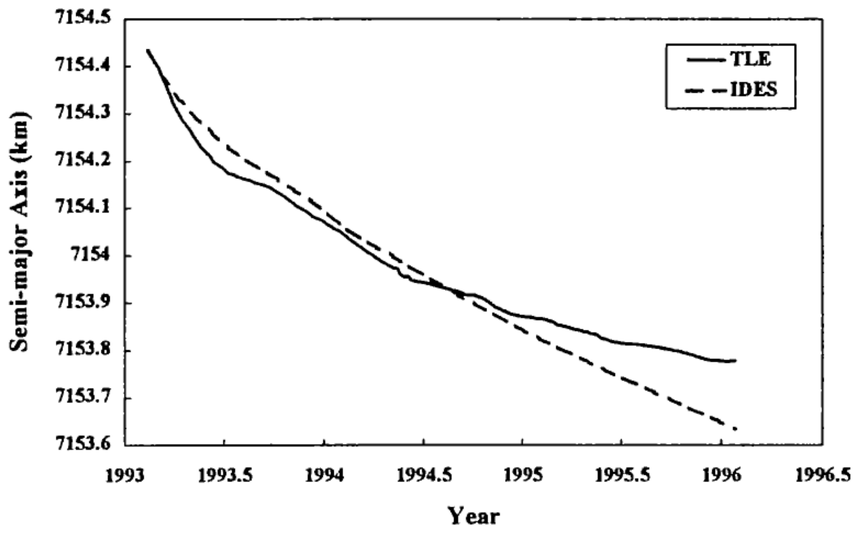

Figure 1. IDES long-term predictions of semi-major axis for Ariane 4-40 stage 3 (1991-050F) in LEO compared to two line element (TLE) data

Figure 1 shows the evolution of semi-major axis for IDES predictions and two line element (TLE) measurements. IDES has very good agreement with TLE data for semi-major axis as it decreases due to atmospheric drag decay with a maximum difference of 0.1 km.

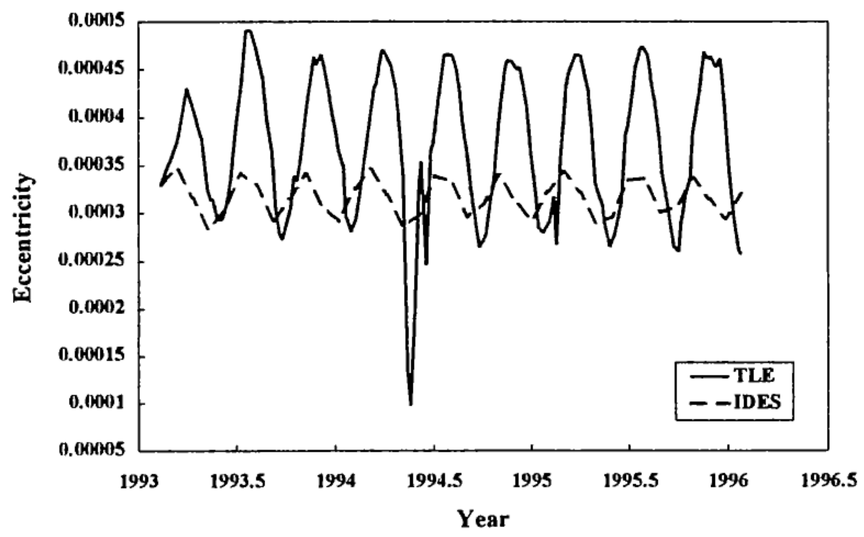

Figure 2. IDES long-term predictions of eccentricity for Ariane 4-40 stage 3 (1991-050F) in LEO compared to two line element (TLE) data

The TLE data in Figure 2 displays periodic fluctuations in the low eccentricity which are modelled accurately by IDES in frequency. However, the magnitude of the fluctuations are slightly smaller for the model predictions. These fluctuations are believed to be due to luni-solar perturbations.

As the second example of orbit evolution we have chosen the Ariane 4-44L stage 3 (COSPAR ID 1992-021C) which was used to launch the Telecom 2B and Inmarsat 2-F4 communications satellites into geostationary orbit (GEO). The upper stage is in a

geostationary transfer orbit (GTO) with high eccentricity and very low inclination. Figure 3 presents the evolution of inclination for this object. The irregular variation of the TLE data between 3° and 4° inclination is followed very closely by the IDES predictions in both shape and magnitude over the 3 year time period. Luni-solar and long period geopotential perturbations are expected to be the main cause of these variations due to the high eccentricity of the orbit.

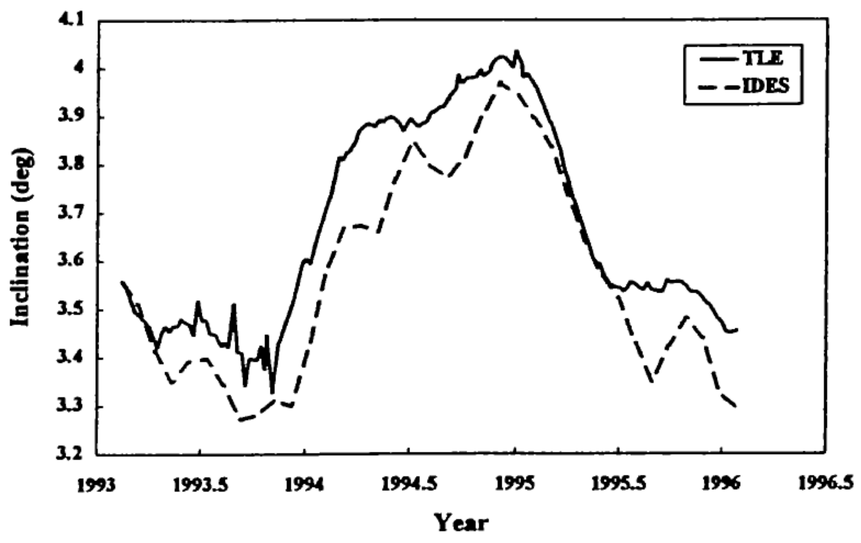

Figure 3. IDES long-term predictions of inclination for Ariane 4-44L stage 3 (1992-021C) in GTO compared to two line element (TLE) data

The accuracy of the IDES breakup model was tested by simulating the fragmentation of the SPOT-1 rocket body in November 1986 at 800 km altitude. The orbital distribution of the simulated debris cloud of >10 cm fragments could be compared to the distribution of tracked fragments from the breakup in ref. 17. However, the tracked fragment data was presented for an epoch 3 months after the event had occurred. Therefore, the validated IDES orbit perturbation model was used to propagate the simulated fragments by this time interval. With a breakup mass of 1634 kg, the breakup model generated 421 fragments which compares well with the catalogued number of 489.

The Gabbard diagrams of Figure 4 and Figure 5 show the distribution of apogee and perigee points over orbital period for the tracked and simulated clouds respectively. The simulated cloud has a very similar distribution to that of the tracked cloud, particularly for orbital periods lower than 97 minutes where fragments have perigee heights deep in the atmosphere at around 300 km. Atmospheric drag causes these fragments to decay, thus lowering their apogee heights and eccentricity before disintegration in the lower atmosphere. Most fragments, however, still remain spread within 200 km above and below the 800 km breakup altitude.

For validating the large-size debris environment, the results of the comparison for the IDES spatial density distribution of >10 cm objects in LEO with the corresponding USSPACECOM catalog distribution are

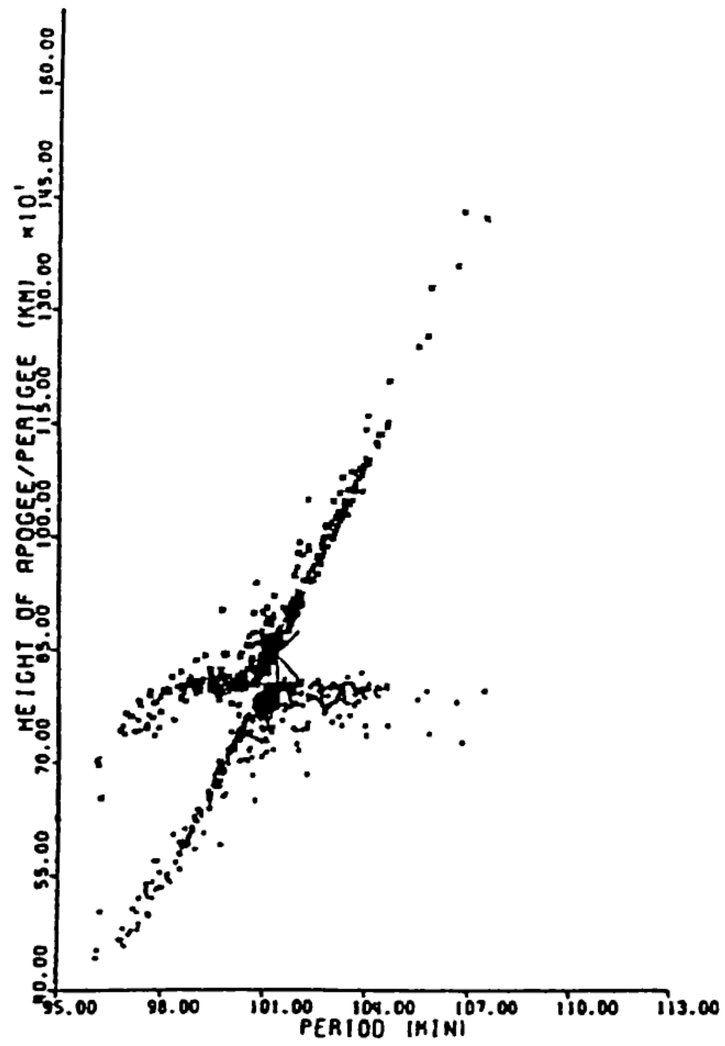

Figure 4. Gabbard diagram of the tracked fragments from the SPOT-1 rocket body breakup - 3 months after the event (ref. 17)

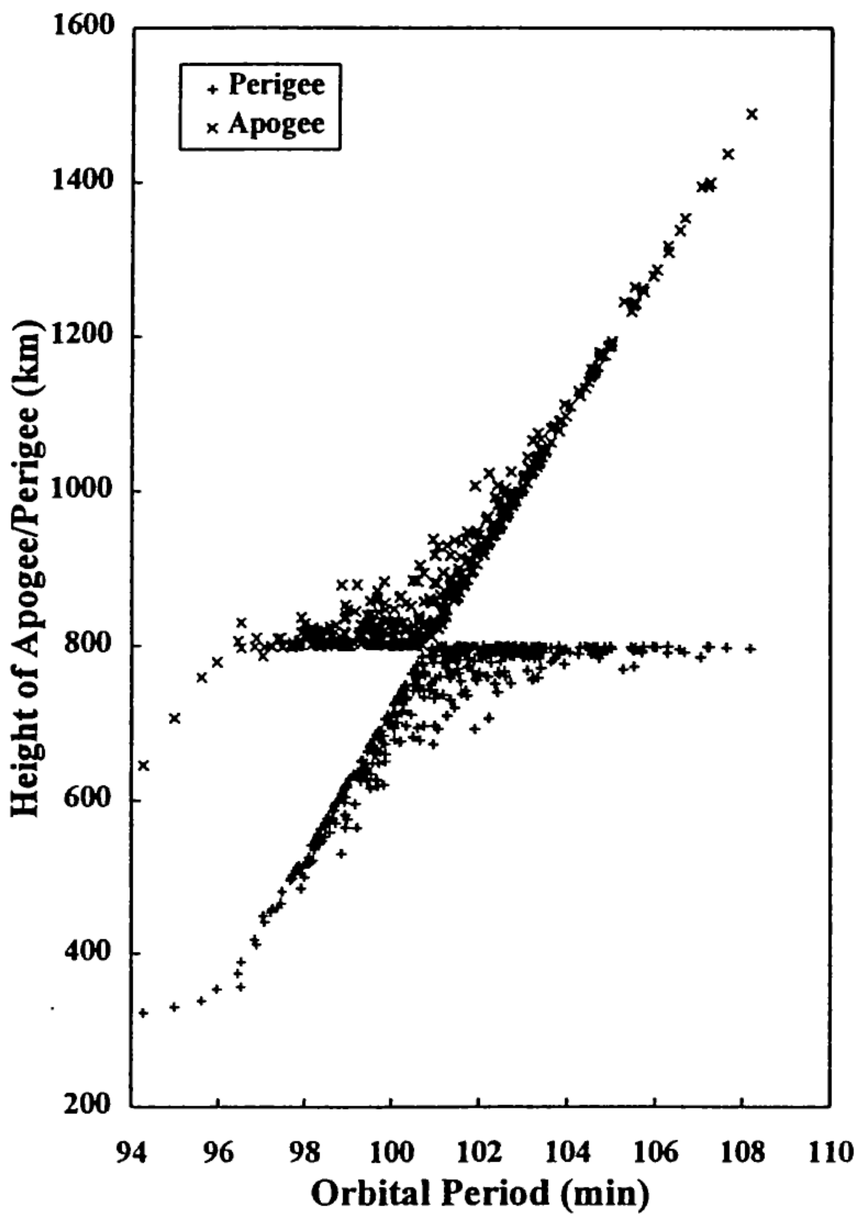

Figure 5. Gabbard diagram for the IDES simulation of the SPOT-1 rocket body fragmentation - 3 months after the event

shown in Figure 6. Both curves display the characteristic peaks in spatial density at 800, 1000, 1400 and 1500 km. The IDES predictions are generally in good agreement with the catalog.

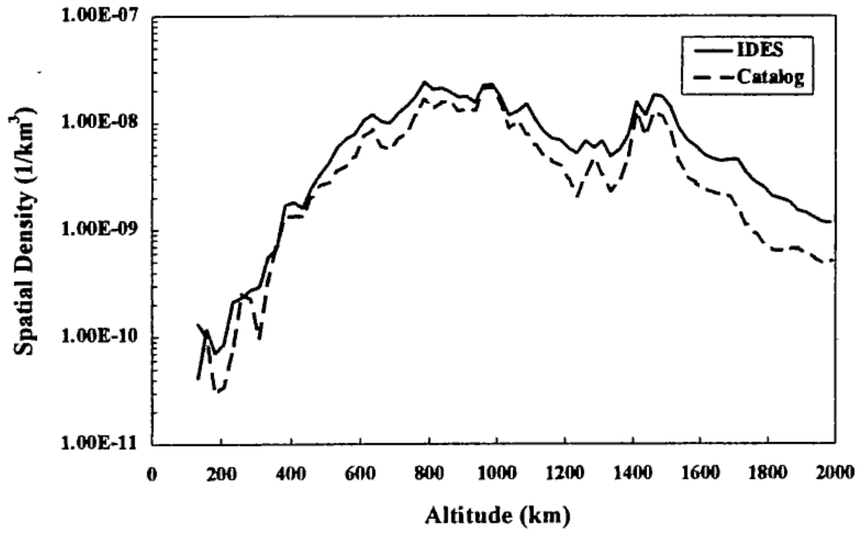

Figure 6. Comparison of IDES >10cm and USSPACECOM catalog spatial density distributions

At some altitudes, particularly above 1000 km, the model predictions are up to a factor of 2 higher than the measured environment. However, the IDES model accuracy is considered to be reasonable since there has been evidence to suggest that the catalog is incomplete (ref. 18) due to the reduced sensitivity of the ground radar sensors for the lower size limit at these higher LEO altitudes. In fact, the lower detection threshold of 10 cm is estimated to increase as altitude increases up to 2000 km. Therefore, some decimetre-sized breakup fragments will not be tracked or catalogued in this region, but the model simulates and includes these breakup fragments in its population.

The IDES >1cm debris environment for 1993 was post-processed by the radar simulation model for the Haystack radar site in 'zenith staring' mode. The predicted detection rate distribution over altitude is compared to the measured distribution in Figure 7. In order to make a direct comparison, the Haystack data is presented for detections of objects larger than 1 cm, rather than for the total data set which also contains detections for debris of a few millimetres.

The plot shows that IDES is in very good agreement with Haystack at altitudes above 1000 km and is a factor of 2 or less over-predicting the detection rate between 600 and 850 km altitude. This is a reasonable agreement considering the possible error margins in Haystack population sampling and the fact that the predictions are for 1993 only and not averaged over the 3 years of observation, which includes the peak solar activity in 1990 and 1991. Between the altitudes of 850 km and 1000 km, the IDES predictions of the population are up to a factor of 5 lower than measured by Haystack. This is because of the recently discovered large population of centimetre-sized spherical objects in 65° inclination circular orbits. These objects are allegedly sodium-potassium coolant droplets leaking from Russian RORSAT spacecraft nuclear reactors (ref. 1). IDES does not currently model this source of debris, although it will be included in the future.

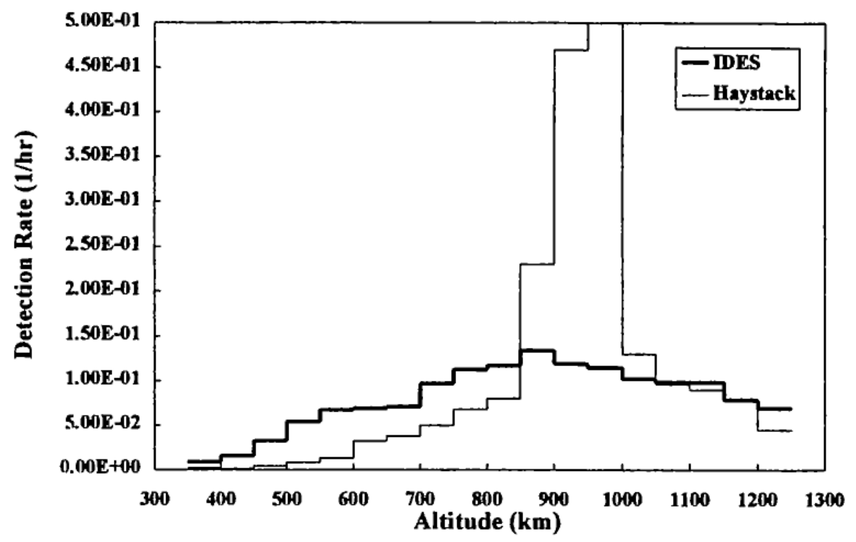

Figure 7. Comparison of IDES predictions and measured detection rates (ref. 1) of debris larger than 1cm in LEO for the US Haystack radar

The comparison of predicted debris impact flux for LDEF averaged over the mission duration with the measured flux for the A11 (52°) forward face (which encountered most of the impacts) is shown in Figure 8.

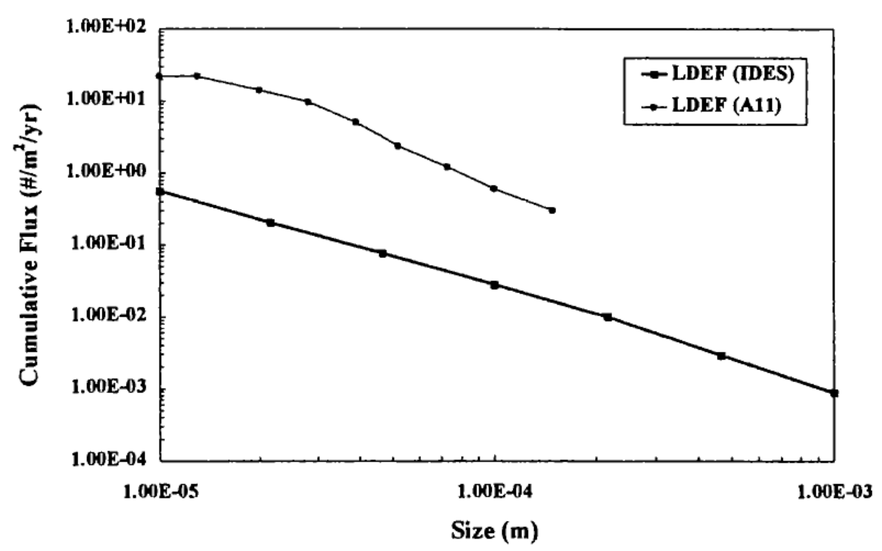

Figure 8. Comparison of size-dependent debris impact flux as predicted by IDES and measured on the A11 (52°) forward face of LDEF (ref. 2)

At a size threshold of 0.1 mm, the IDES predictions are an order of magnitude lower than the measurement data and at the lower size of 10 microns, this under-prediction increases to a factor of 40. This significant discrepancy can be explained by the possible under-prediction of breakup models, but more importantly due to the lack of modelling paint flakes and other particles which are generated by the surface degrading action of atomic oxygen erosion, thermal cycling, and UV radiation. These debris particles are known to be present at very small sizes in the LEO environment. By modelling the surface degradation mechanisms, it may be possible to narrow the model under-prediction of small-size debris impact fluxes.

5. CONCLUSIONS

1.) The IDES orbit perturbation model and breakup model show good accuracy when compared to the orbital evolution of rocket bodies and breakup distributions from the USSPACECOM catalog.

2.) The IDES >10cm debris environment for 1996 shows a good agreement with the USSPACECOM catalog environment, except at altitudes above 1000 km where IDES is a factor of 2 higher than the catalog.

3.) The IDES >1cm debris environment produces detection rates in the Haystack radar beam that are similar to the measured rates between 700 and 850 km, and above 1000 km. There are large under-predictions by IDES around 900 to 1000 km because IDES does not yet model the suspected RORSAT droplet debris source.

4.) The IDES debris environment >0.1mm produces an impact flux relative to LDEF that is a factor of 10 below the measured LDEF flux. At 10 micron sizes, the gap increases to a factor of 40. This is mainly because IDES does not yet model micro-debris from atomic oxygen, thermal cycling and UV effects on exposed surfaces.

6. REFERENCES

1. Reynolds, R., Matney, M., A Comparison of Haystack Radar Measurements with EVOLVE Debris Environment Predictions, Paper IAA-95-IAA.6.3.08, *46th International Astronautical Congress*, Oslo, Norway, October 1995.

2. Hörz, F., Bernhard, R.P., See, T.H., Brownlee, D.E., Natural and Orbital Debris Particles on LDEF's Trailing and Forward-Facing Surfaces, *LDEF - 69 Months in Space, Third Post - Retrieval Symposium*, NASA CP 3275 Part 1, pp. 415-429, November 1993.

3. Walker, R., Hauptmann, S., Crowther, R., Stokes, H., Cant, A., Introducing IDES: Characterising the Orbital Debris Environment in the Past, Present and Future, AAS 96-113, *Advances in the Astronautical Sciences*, Space Flight Mechanics 1996, Vol. 93 Part I, pp. 201-220, 1996.

4. Madler, R.A., Sensitivity of the Near-Earth Orbital Debris Environment to Satellite Fragmentation Parameters, *PhD thesis, University of Colorado*, 1994.

5. Rossi, A., A. Cordelli, C. Pardini, L. Anslemo, P. Farinella, Modelling the Space Debris Evolution: Two New Computer Models, AAS 95-186, *Advances in the Astronautical Sciences*, Space Flight Mechanics 1995, pp. 1217-1231, 1995.

6. Roy, A.E., *Orbital Motion*, Third Edition, 1988.

7. King-Hele, D.G., *Satellite Orbits in an Atmosphere: Theory and Applications*, Blackie, 1987.

8. Cook, G.E., Luni-Solar Perturbations of the Orbit of an Earth Satellite, *RAE Technical No. G.W. 582*, 1961.

9. Space Station Freedom Program Office, Space Station Natural Environment Definition for Design, Revision A, *SSP 30425*, Reston VA, June 1991.

10. Jehn, R., Fragmentation Models, *ESOC/MAS Working Paper* 312, ESOC, Darmstadt, December 1990.

11. Reynolds, R., Documentation of Program EVOLVE: A Numerical Model to Compute Projections of the Man-Made Debris Environment, *System Planning Corporation report* OD91-002-U-CSP, 1991.

12. McKnight, D., R. Maher, L. Nagl, Refined Algorithms for Structural Breakup Due to Hypervelocity Impact, *Hypervelocity Impact Society Symposium*, Sante Fe, NM, Oct.16-20 1994.

13. Su, S.-Y., D.J. Kessler, Contribution of Explosions and Future Collision Fragments to the Orbital Debris Environment, *Advances in Space Research*, Vol. 10, No.2, p. 25-34, 1985.

14. Reynolds, R.C., A Review of Orbital Debris Environment Modelling at NASA/JSC, *Orbital Debris Conference,* AIAA-90-1355, Baltimore, MD, Apr. 16-19 1990.

15. Ojakangas, G.W., P. Anz-Meador, R. Reynolds, Orbital Debris Environment, AIAA 90-3863, *AIAA Space Programs and Technologies Conference*, Huntsville AL, September 1990.

16. Klinkrad, H., Collision Risk Analysis for Low Earth Orbits, *Advances in Space Research*, Vol. 13, No. 8, pp. 177-186, 1993.

17. Nauer, D.J., History of On-Orbit Satellite Fragmentations, 7th Edition, *Teledyne Brown Engineering*, July 1993.

18. Henize, H., Stanley, J., Optical Observations of Orbital Debris, paper AIAA-90-1340, *AIAA/NASA/DOD Orbital Debris Conference*, 1990.